Poly-condensation of N-(2-acetamido)-2-aminoethanesulfonic acid with formaldehyde for the synthesis of a highly efficient sorbent for Cs(I)

Mohammed Hamza, Guibal Eric, Khalid Althumayri, Yuezhou Wei, Ahmed Eid, Amr Fouda

Poly-condensation of N-(2-acetamido)-2-aminoethanesulfonic acid with formaldehyde for the synthesis of a highly efficient sorbent for Cs(I)

Mohammed F. Hamza [a,b], Eric Guibal [c,*], Khalid Althumayri [d], Yuezhou Wei [a,e,*], Ahmed M. Eid [f], Amr Fouda [f]

[a] School of Nuclear Science and Technology, University of South China, Heng Yang 421001, China
[b] Nuclear Materials Authority, POB 530, El-Maadi, Cairo, Egypt
[c] Polymers Composites and Hybrids (PCH), IMT Mines Ales, Alès, France
[d] Department of Chemistry, College of Science, Taibah University, 30002 Al-Madinah Al-Munawarah, Saudi Arabia
[e] School of Nuclear Science and Engineering, Shanghai Jiao Tong University, Shanghai, China
[f] Botany and Microbiology Department, Faculty of Science, Al-Azhar University, Nasr City, Cairo 11884, Egypt

ARTICLE INFO

Keywords:
Easy synthesis of a highly efficient sorbent for cesium through ready condensation of acetamido-aminomethanesulfonic acid (via formaldehyde reaction)
Fast cesium uptake onto microparticles (fitted by the pseudo-first order rate equation)
Remarkable desorption and sorbent recycling using 0.3 M HNO_3 solution
Good sorption performance in seawater
Selectivity against alkali and alkali-earth metal ions
Limited toxicity against Gram+ and Gram- bacteria and pathogenic yeast, reduced cytotoxicity against normal cells (but inhibiting cancerous cells)

ABSTRACT

A new sorbent (ACES-F micro-particles) is readily synthesized by the one-pot reaction of N-(2-acetamido)-2-aminoethanesulfonic acid with formaldehyde (poly-condensation reaction). The mesoporous sorbent is characterized by BET analysis (S_{BET}: ≈6 $m^2 g^{-1}$), SEM-EDX (N: ≈7–8 % and S: 5 %), FTIR spectroscopy (identification of amine, sulfonic groups and their interactions with metal ions), TGA, elemental analysis, and titration (pH_{PZC}: ≈5.7). The study of pH effect on Cs(I) shows an optimum close to 8 (with intermediary optimum at pH 4, associated with different reactive groups). The micron-size sorbent shows fast sorption (equilibrium in 60 min) and the pseudo-first order rate equation fits the kinetic profile. The sorption isotherm reaches up to 1.99 mmol Cs g^{-1}; the Langmuir equation models isotherm profiles. The sorption decreases with increasing temperature; sorption is exothermic. Cesium uptake is affected by the presence of NaCl; however, even in large excess of salt (i.e., 4 M) sorption remains relatively high (loss <60 %). Selectivity is confirmed by the remarkable preference of the sorbent for Cs against alkali and other competitor metal ions, especially at pH_{eq} ≈7. Metal desorption is highly effective using 0.3 M HNO_3 solutions: complete desorption occurs in 30 min. The sorbent can be recycled for at least five cycles (losses <3 %). The interest of ACES-F for cesium recovery from seawater is confirmed by the study of Cs(I) sorption (and other major elements) from Vietnam and Egypt samples. The safety of the sorbent for aqueous bodies is evaluated by the cytotoxicity of the sorbent (limited against normal cells but highly reactive for cancerous cells); while the sorbent shows interesting antimicrobial properties for Gram+, Gram- and pathogenic yeast.

1. Introduction

Apart its few uses in industry as drilling fluids, special optical glass, catalyst promoter, atomic clock, or in radiation monitoring equipment, cesium is mainly investigated as one of the most representative of the hazardous elements in the suite of nuclear fission products (as its radioactive isotopes: ^{134}Cs, ^{135}Cs, and ^{137}Cs) [1]. This is one of the main motivations for the numerous studies developed for the last decades.

Solvent extraction has been recognized as an efficient process for the recovery of cesium, especially for high concentrations and nuclear power effluents [2,3]. However, for diluted solutions, combined treatments involving sorption processes are usually more appropriate. Extractant-impregnated supports constitute an intermediary step between solvent extraction and solid/liquid systems in the design of sorbents [4–6]. Zeolites and clays [1,7–10] have been widely used for accumulating cesium based on cage effect. This cage-effect can be also used with Prussian-blue (and analogues) supported materials [11–17] or metal–organic frameworks (MOFs) [18]. Ion-exchange and chelating resin are conventional systems for the recovery of metal ions (including Cs(I) and Sr(II) [19,20]. By analogy with commercial and in-development resins, biosorption processes were also investigated for cesium removal from aqueous solutions, including algal biomass

* Corresponding authors.
E-mail addresses: m_fouda21@usc.edu.cn (M.F. Hamza), eric.guibal@mines-ales.fr (E. Guibal), kthumairi@taibahu.edu.sa (K. Althumayri), yzwei@usc.edu.cn (Y. Wei), aeidmicrobiology@azhar.edu.eg (A.M. Eid), amr_fh83@azhar.edu.eg (A. Fouda).

[21,22], microalgae [23], cyanobacteria [24], biopolymers [25], or agriculture wastes [26]. Recently, Lee et al. [27] reported the use of sulfonic Dowex G26 cation exchange resin for the sorption of Cs(I), including in complex effluents such as brines. This is in the continuity of previous studies reporting the interest of sulfonate-bearing resins [28–30]. Different methods have been used for preparing these sulfonic-based resins, including radiation-induced polymerization (sodium styrene sulfonate with polyacrylamide, [31]), chlorosulfonation of styrene-divinyl benzene beads (followed by grafting of aminopyridine, [32]), or Friedel-Crafts alkylation routes (for synthesis of sulfonated hyper-cross-linked polymers, [33]).

Herein, a new sulfonic acid-bearing resin is designed by poly-condensation of a precursor (i.e., N-(2-acetamido)-2-amino-ethanesulfonic acid, ACES) in the presence of formaldehyde, in mild acidic conditions. This type of reaction has been shown to be efficient for designing polymeric sorbents [34,35]. This simple one-pot synthesis method allows producing a multifunctional sorbent bearing amine, amide, and sulfonic reactive groups (herein called ACES-F; which may broadly contribute to metal binding. The objective of this work focuses on the evaluation of the potential of this sorbent for the recovery of Cs(I) under different conditions of pH (mild acidic solutions, i.e., pH 4, vs mild alkaline conditions, i.e., pH 8). A special attention is also paid to the determination of selectivity properties in order to estimate the potential of this new sorbent for the treatment of complex solutions (including seawater or brines). For this purpose, the sorbent is fully characterized in terms of physical and chemical properties, before investigating the sorption characteristics using standard methodologies including the study of pH effect, uptake kinetics, sorption isotherms (at different temperatures for analyzing thermodynamics), metal desorption, sorbent recycling and selectivity (against metal ions and in function of ionic strength). Finally, the sorbent is tested for Cs(I) removal from complex solutions (i.e., seawater). Apart this study of sorption properties, the antimicrobial properties, and toxicity of the new material are characterized by the evaluation of the ZOI (zone of inhibition, with well technique) and the cell viability test, respectively.

2. Materials and methods

2.1. Materials

Cesium nitrate ($CsNO_3$; 99 %), N-(2-acetamido)-2-amino-ethanesulfonic acid (≥99.9 %), strontium nitrate (99.99 %), calcium chloride ($CaCl_2$ ≥ 99.9 %), sodium hydroxide (NaOH: ≥97.0 %), and formaldehyde (37 %) were purchased from Sigma-Aldrich (Taufkirchen, Germany). Magnesium chloride ($MgCl_2{\cdot}6H_2O$, 99 %), sodium chloride (NaCl, ≥99.98 %), aluminum chloride ($AlCl_3{\cdot}6H_2O$; 95 %), ferric chloride, ($FeCl_3$, ≥99.5 %) and acetic acid (glacial, ≥99 %) were supplied by Guangdong Guanghua, Sci Tech-Co., Ltd (Guangdong,China).

2.2. Synthesis of ACES-F

The precursor (i.e., N-(2-acetamido)-2-aminoethanesulfonic acid, 7.5 g) was dissolved in 25 mL of demineralized water (in 100-mL three necks round flask, equipped with a condenser, agitator, and thermometer). Formaldehyde (3.7 mL, ≈4.03 g, 37 % w/w solution) was dropped into the reactor. The pH of the mixture was adjusted to 4, using 0.5 mL glacial acetic acid. The mixture was reflux at 90 °C for 5 h, under vigorous agitation (velocity 190 rpm). The white yellowish precipitate was filtered and washed up with acetone before being air-dried overnight at 60 (±5) °C. The final product (9.4 g) was called ACES-F. Scheme 1 shows the tentative structure of ACES-F. Based on the mass increase (compared with the amounts of precursor and condensation agent), the yield for sorbent production was close to 82 %.

2.3. Sorbent characterization

The FT-IR spectra were performed for raw material, after sorption, after being treated with simulated solutions of loading and elution (in terms of pH or acidic solution), and after recycling for 5 cycles of sorption/desorption. The samples were dried at 60 °C for 24 h before grinding and pelletizing with KBr to produce KBr-disks. The spectra were collected using an IR-Tracer; 100 FT-IR spectrometer (Shimadzu, Tokyo, Japan). The pH_{PZC} (pH of zero-charge) was determined using the pH-drift method: an amount of 100 mg of sorbent was added to 50-mL of 0.1 M NaCl solutions (as background salt) with variable initial pH values (in the range 1–11). The mixture was agitated for 48 h and the final pH (pH_f) was measured. The pH_{PZC} is referred to the pH value corresponding to $pH_0 = pH_f$ (no pH variation after contact with the sorbent). The pH values were monitored using of S220-Seven compact pH-ionometer (Mettler-Toledo Instruments, Shanghai, China).

The concentration of cesium in the solutions was determined using atomic absorption spectrometry (Unicam 969, Thermo Electron-Corporation, Waltham, MA-USA). The concentration of sodium in the solution was determined by flame atomic absorption (FAAS, AA-7000-Shimadzu, Tokyo, Japan, while other elements in the solution (i.e., Fe, U, As, Al, Sr, etc.) were determined by ICP-AES (inductively coupled plasma atomic emission spectrometer, ICP 7510-Shimadzu, Tokyo, Japan). Theses samples were filtrated through filter membrane (pore size 1.2 μm) prior analysis.

The SEM analysis was performed with a Phenom ProX scanning electron microscope (ThermoFisher Scientific, Eindhoven, Netherlands). The chemical composition of the materials semi-quantitatively determined using EDX tool (energy dispersive X-ray analysis coupled with the SEM). The porosity and surface area of the sorbent were characterized

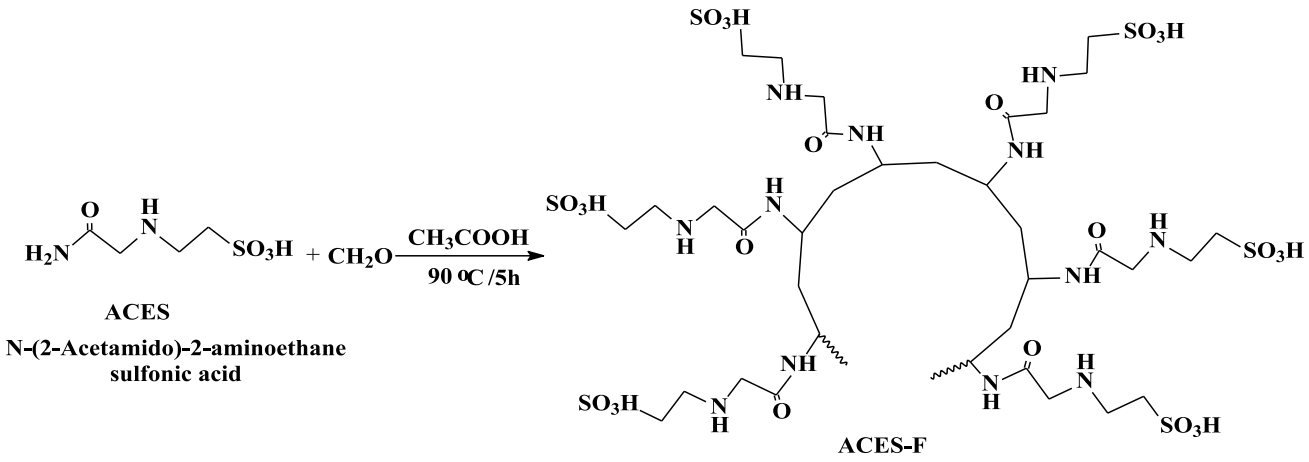

Scheme 1. Synthesis procedure for the preparation of ACES-F sorbent.

by evaluation of nitrogen adsorption/desorption isotherms using TriStar II Micromeritics analyzer (Norcross- GA, USA). The BET equation was used for the determination of the specific surface area, while the porous characteristics were obtained by application of BJH equation, for both adsorption and desorption branches. The sample was swept in the nitrogen gas for around 4 h at 130 °C. Thermogravimetric analysis was carried out using the TG-DTASTA: 449-F3, Jupiter TG-DTA (Netzsch, Gerätebau-HGmbh, Selb, Germany). Analysis was performed under N_2 atmosphere with 10 °C min^{-1} temperature ramp.

The elemental composition (C, S, N, H and O, weight contents) was carried out on the sorbent using element analyzer (CHNOS, Vario EL III, Elementar Analysensysteme GmbH, Langenselbold, Germany). In addition, two titration procedures were tested for quantifying the amount of sulfonate groups present on the sorbent:

(a) 20 mL 1 M NaCl solution were mixed with the sorbent (m: 0.1 g) under stirring for 5 h. A volume of 10 mL of free solution was collected for titration using 1 M NaOH solution (with phenolphthalein as the indicator). The volume of titrating alkaline solution (i.e., 2.4 mL) is readily converted into sulfonate content: 4.8 mmol -SO_3 g^{-1} [36].

(b) 10 mL 1 M NaOH solution was mixed with the sorbent (m: 0.1 g) for 5 h, under stirring. After filtration, the residual solution was titrated against HCl (1 M, 5.1 mL). The back-titration of sulfonate groups corresponds to 4.9 mmol -SO_3 g^{-1} (consistently with the first method) [37].

2.4. Study of sorption properties and modeling

Experiments were performed in batch. A fixed volume of solution (V, L), at initial concentration (C_0, mmol Cs L^{-1}) and fixed initial pH_0, was mixed with a given amount of sorbent (m, g). After selected time (24–48 h for equilibrium experiments, or variable time for uptake kinetics), samples were collected and filtrated (filter membrane, pore size: 1.2 μm) before being analyzed for residual metal concentration (C_{eq}, mmol Cs L^{-1}). The concentration of the metal in the sorbent (q_{eq}, mmol Cs g^{-1}) was calculated by the mass balance equation: $q_{eq} = (C_0\text{-}C_{eq}) \times V/m$. The determination ratio (D, L/g) was obtained as the equilibrium ratio: $D = q_{eq}/C_{eq}$. For desorption tests, the samples collected at the end of uptake kinetics were used for investigating desorption kinetics and sorbent recycling. The experimental procedures were similar to those adopted for uptake kinetic using 0.3 M HNO_3 solutions as the eluent. Experiments were duplicated, and figures represent the average value with the standard deviation. The remarkable superposition of experimental series confirm the good reproducibility of sorption tests. Sorption tests were also performed on synthetic complex solutions (multi-metal equimolar solutions, and in presence of increasing amounts of NaCl) with similar procedures to evaluate the sensitivity of the sorption properties to environmental and competition parameters. The specific experimental conditions are systematically reported in the caption of the figures.

The modeling of uptake kinetics and sorption isotherms use conventional equations, which are summarized in Supplementary Information (SI, Section A, Tables S1a and S1b). Kinetic profiles were fitted by the pseudo-first and pseudo second order rate equations (PFORE and PSORE), and by the Crank equation (for resistance to intraparticle diffusion, RIDE) [38–40]. The sorption isotherms were simulated using the Langmuir, Freundlich, Sips, and Temkin equations [38,41,42]. The quality of the fits was evaluated by the determination coefficient (i.e., R^2) and the Akaike Information Criterion (AIC, [43]).

2.5. Application to seawater

Sorption tests were also performed for recovering selected metals from real seawater samples collected in Da Nang (Vietnam) and Ra's Garb (Red Sea Egypt). This part of the study completes the investigation of sorption selectivity with very complex effluent (large excess of sodium chloride). These experimental conditions simulate the possible application of the sorbent for the treatment of a cesium-contaminated seawater; as a pre-evaluation of the potentiality for ACE-F use in case of nuclear incident.

2.6. Antimicrobial properties of ACES-F sorbent and cytotoxicity

The use of newly synthesized materials must be questioned in terms of the impacts of their application onto the environmental and biological bodies. Herein, two criteria were investigated considering (a) the antimicrobial properties (against two Gram-positive, two Gram-negative bacterial strains, and a unicellular fungus), and (b) the cytotoxicity of ACES-F (against two normal cell lines and one carcinogenic cellular cell line). The experimental procedures are fully described in the SI (Section E).

3. Results and discussion

3.1. Sorbent characterization

3.1.1. Morphology and textural properties

Fig. S1 shows the SEM micrographs of ACES-F sorbent particles before and after cesium binding. The semi-quantitative EDX analyses of the surface of these samples are also provided. Sorbent particles are irregular in shape and size. The particles are generally rounded with sharp and irregular edges; meaning that external surface is higher than for smoothed surfaces. The size of these micro-objects is varying in the range 8–15 μm. After cesium sorption, the particles appear agglomerated. The semi-quantitative EDX analysis of the surface of the sorbents shows comparable atomic concentrations for C and O elements (46.1 % and 41 %, respectively) but also substantial amounts of N and S elements (7.2 % and 5.5 %, respectively). The EDX analysis confirms the affinity of the sorbent for Cs(I); after sorption, the atomic content reaches 2.3 %.

The textural properties of ACES-F are summarized in Fig. S2. The sorbent is relatively poorly porous (porous volume around 0.0178–0.0209 cm^3 g^{-1} (derived from the adsorption and desorption branched for setting the extremum values), with the average size of pores ranging between 171 Å (sorption branch of N_2 sorption/desorption isotherms) and 129 Å (desorption branch), both using the BJH method. According to IUPAC nomenclature, the sorbent may be qualified a mesoporous material. This may explain that the specific surface area of ACES-F is relatively weak (i.e., 4.54 m^2 g^{-1}, by the BET method; the C-value is found close to 27.12). The N_2 adsorption/desorption isotherms correspond to type IV physisorption profiles (also correlated to mesoporous structure, [44]). The hysteresis loop approaches the H3 shape; Thommes et al. [44] reported that this type of shape is usually associated with non-rigid aggregates of plate-like particles and also porous network consisting of macropores not completely filled with pore condensate.

3.1.2. FTIR characterization

FTIR spectra are collected and discussed in Section B.2. In order to evaluate and separate the respective contributions of environmental parameters (pH control, or contact with eluent) and proper interaction of the sorbent with Cs(I) at pH 4 and pH 8, the changes observed on FTIR spectra are compared for samples mixed with solutions at pH 4 and 8 in the presence and absence of Cs(I). The main changes observed at pH 4 concern carbonyl and nitrogen-based reactive groups and the weak shift of the band of sulfonic-based groups (and the appearance of strong peak at 1385 cm^{-1}, which can be associated with nitrate ions from the solution). Cesium sorption, at this pH, mainly involve carbonyl and amine groups. In the case of pH 8, the peak at 1111 cm^{-1} is significantly reduced (compared with pH 8-conditioned sorbent and pristine ACES-F); this band may be assigned to an amine group but may be also associated with the asymmetric stretching vibration of SO_3. Other *N*-based and/or C—S bonds are affected by cesium sorption (shift of the band from 617 to 679 cm^{-1}). A new band (actually a doublet) also appears at 930 cm^{-1} after cesium binding for C—O stretching (which is associated with the tautomerization of amine groups in alkaline solutions). The

shift of the carbonyl band (from 1730 cm^{-1} to 1742 cm^{-1}) also demonstrates that the chemical environment of > C=O is also involved in metal sorption. At neutral (weakly basic) pH, cesium sorption influences the environment of carbonyl and amine-based groups. In addition, sulfonic groups (deprotonated, consistently with the acidic behavior of sulfonic acid groups and pH_{pzc} values) are also involved in metal binding. These supplementary groups (associated with the deprotonation of sulfonic acid moieties) contribute to the gap in sorption capacity at pH 4 and at pH 8 (see below, Section 3.2.1.).

3.1.3. Thermogravimetric analysis

Fig. S6a shows that the thermal degradation of the polymeric sorbent operates in three steps:

(a) below 203.4 °C, the sorbent loses about 14 % of its weight, associated with water release,

(b) in the range 203.4–372.6 °C, the weight loss represents 47 %, this is probably associated with the depolymerization of the sorbent and the degradation of ending groups (S-bearing and *N*-bearing groups),

(c) above 372.6 °C, the weight loss reaches 32 % and corresponds to the formation and progressive degradation of the char (above 450 °C). It is noteworthy that the char is relatively stable; indeed, above 600 °C, the additional weight loss remains negligible.

At 890 °C, the total weight loss reaches 92.9 %. The DTG (illustrated by Fig. S6b) shows two important transitions occurring at 347.0 °C and 490.4 °C (with two weaker shoulders at 141.6 °C and 594.2 °C).

3.1.4. Elemental analysis

Table S3 reports the elemental analysis of the sorbent (compared with the theoretical analysis of ACES precursor). The reaction of formaldehyde with amine-based reagents (such as urea, a carbamide-based compound) is supposed to involve addition reaction to form for example methylolurea (case of urea), followed by a polycondensation reaction through ether or methylene links. This reaction leads to a relative increase of C content into the produced polymer. This is confirmed by elemental analysis: C content increases from ≈22.0 mmol C g^{-1} in ACES to ≈26.4 mmol C g^{-1} in ACES-F. As expected, the O content hardly changes after polymerization (≈24.4 vs ≈22.0 mmol O g^{-1}). However, unexpectedly the fraction of N element in the material is significantly reduced (from ≈11 to ≈6.5 mmol N g^{-1}): this halved content cannot be correlated to the weight variation associated with the insertion of formaldehyde residue in the poly-condensed material. This probably means that a more complex mechanism is involved (compared to urea/formaldehyde polycondensation route). It is noteworthy that S content reaches 3.14 mmol S g^{-1} (this is less than the content in ACES; i.e., 5.49). However, it is consistent with N content; indeed, N/S molar ratio in ACES (i.e., 2) is close to the value found in ACES-F (i.e., 2.07). The sulfonate content (determined by titration) on ACES-F can be evaluated to ≈4.8 mmol -SO_3 g^{-1}.

3.1.5. Titration – pH_{PZC}

The titration curve (pH-drift method) of the sorbent was performed in two types of solutions (i.e., 0.1 M and 1 M NaCl-containing background solutions). Fig. S7 shows relatively good superposition of the curves with a pH_{PZC} close to 5.58–5.75. It is noteworthy that N-(2-acetamido)-2-aminoethanesulfonic acid (ACES, also known as N-(carbamoylmethyl)taurine) is qualified a good buffer reagent (pK_a: 6.9). The polycondensation (in presence of formaldehyde) decreases by more than one pH unit through the transition between positively charged and deprotonated material. Apparently, the titration curve shows an inflexion point (at least a break) in the slope around 6.5–7; in a region where the sorbent is negatively charged. Notably, ACES may be converted into 2-[(2-amino-2-oxoethyl)ammonio]ethanesulfonate by tautomerization (deprotonation of sulfonic acid group into sulfonate group with proton transfer to central amine group, see SI, Section B4). The higher positively charged surface is registered at pH_{eq} 3.7–3.8, while the surface turns to negatively-charged material at pH above 5.7. The protonation/deprotonation of reactive groups (depending on pH vs pH_{PZC}) may control attraction/repulsion phenomena for the binding of target metal ions.

3.2. Sorption properties

3.2.1. Effect of pH

The effect of pH on Cs(I) sorption using ACES-F is compared at T: 20 and 50 °C in Fig. 1. In strongly acidic solution (i.e., pH close to 1), the strong protonation of the sorbent (and the competition of protons) limits the sorption of cesium. Incrementing the pH of the solution progressively increases the sorption of cesium up to pH_{eq} close to 7.9, where the sorption capacity tends to stabilize. Increasing the temperature (from 20 to 50 °C) halves the sorption capacity (from 1.094 ± 0.028 to 0.553 ± 0.026 mmol Cs g^{-1}): the sorption is exothermic. It is noteworthy that the pH-edge curve shows a double-wave profile. The triplicate experiments systematically showed the same behavior: the repeatable experiments confirm that a first step can be observed at pH 4–5 (slope break) followed by a new increasing step up to pH 8. This two-steps profile is less marked in the case of T: 50 °C. The pH may influence metal sorption through the effect on metal speciation and/or the impact of protonation/deprotonation of sorbent. Herein, under selected experimental conditions Cs(I) is present as free cesium (i.e., Cs^+) between pH 2 and pH 9 (Cs(I) percentage >99 %); at pH 1, the solutions contain a small fraction of $CsNO_3$ (i.e., 7.4 %) (Fig. S8). However, in the current case, the relative stability of Cs(I) speciation in the investigated pH range does not influence the sorption process (as it may occur with systems involving pH-variation of metal speciation). Therefore, the large variation in sorption cannot be attributed to metal speciation; it is thus protonation and deprotonation of reactive groups that influence metal binding. The expected structure of ACES-F suggests the presence of both basic amine/amide groups and sulfonic acid groups, which behave in opposite ways regarding the effect of pH. Sulfonic acid-based groups are strong cationic exchange groups (with very low pK_a values), while amine/amide groups are weakly basic groups (with much higher pK_a values). In the primary pH region (i.e., below pH 5, global cationic charge brought by protonated amine groups), sulfonate groups bind Cs(I) with progressive decrease in the competition effect of protons. When the pH increases above pH 5, the amine/amide groups progressively deprotonate; this deprotonation, in turn, brings to the sorbent new reactive groups for cesium binding and the sorption capacity increases again. Above pH 8, the stabilization of sorption capacity (including a weak decrease more marked at T: 50 °C) can be explained by a shielding effect. Similar behavior was reported for the binding of Sr(II) metal cations onto amidoximated sorbents [45,46].

Table S4 reports Cs(I) sorption performances for a series of sorbents, including the optimum pH. Selected pH values range between 5 and 9 (with most in the range 7–8). For those sorbents accepting the acidic solutions (i.e., pH 5), the sorption capacity remained below 1.1 mmol Cs g^{-1}; meaning significantly lower than the value reached at pH 4 with ACES-F (1.44 mmol Cs g^{-1}, at saturation of the sorbent, see below Section 3.2.3.).

Fig. S9 shows the $\log_{10}$ plot of distribution ratio D (L/g; $D = q_{eq}/C_{eq}$) vs the equilibrium pH. This plot logically confirms the negative impact of the temperature on cesium recovery: D is shifted toward lower values when T increases up to 50 °C. Another interesting information concerns the substantial increase in the shift at the higher pH values (consistently with Fig. 1). Assuming that in this pH region the amine groups are contributing to cesium binding, this could indicate that these amine groups are more sensitive to temperature than sulfonate groups.

The pH variation during metal sorption at both T: 20 °C and 50 °C appears in Fig. S10. The triplicate experiments show good reproducibility and that pH variations are independent of the temperature. Between pH 1 and 4, the equilibrium is not significantly affected by metal binding. On the opposite hand, above pH 4 the equilibrium pH tends to progressively decrease; this pH decrease becomes relatively important

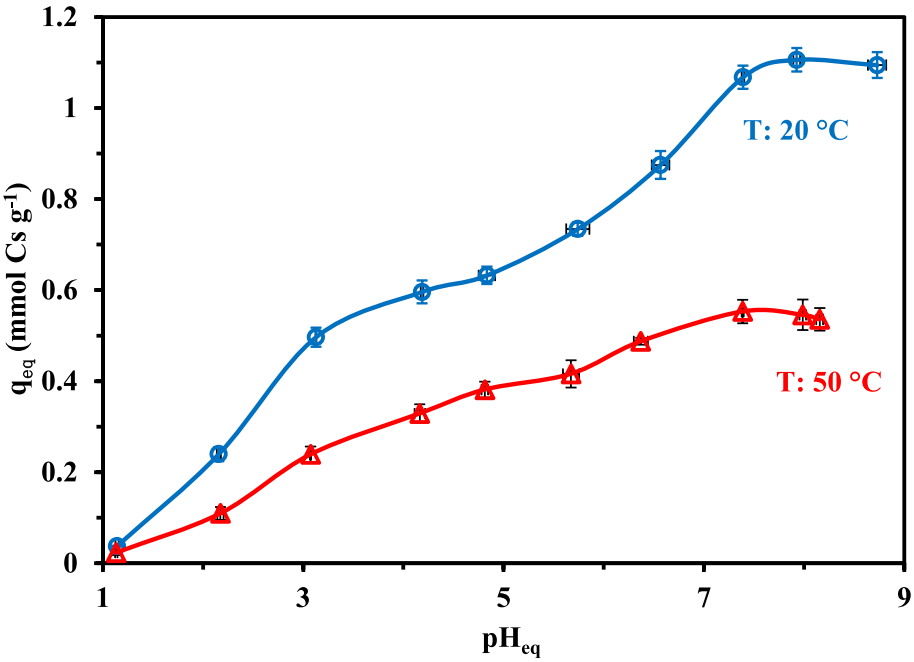

Fig. 1. Effect of pH on Cs(I) sorption capacity using ACES-F sorbent at T: 20 °C and 50 °C (Sorbent dose, SD: 0.67 g/L; time: 48 h; v: 210 rpm; C_0: 0.767 ± 0.039 mmol Cs L^{-1}; average (+/− standard deviation) for triplicated series).

above pH_0 6 and may reach up to 1.8 unit when pH_0 = 10. This is consistent with the strong pH variation observed in the determination of pH_{PZC} value (pH shift was more marked above pH_{PZC}). With increasing the pH, the sorbent is naturally deprotonated; in addition, in the presence of Cs(I), metal binding releases protons.

Scheme 2 illustrates the suggested mechanisms occurring in the sorption of uranyl ions at pH 4 and pH 8. These hypotheses are supported by the effect of the pH and the FTIR characterizations.

3.2.2. *Uptake kinetics*

The study of pH effect has singularized two specific values of pH (probably associated to sulfonate and amine groups). Therefore, uptake kinetics have been compared at two specific pH values (i.e., pH 4 and 8) (Fig. 2). The limited values of standard deviation confirm the good reproducibility of sorption tests. A contact time of 60–90 min is sufficient for reaching the equilibrium at pH 8, under selected experimental conditions. It is noteworthy that at pH 4, the sorption is reduced (consistently with the data collected in Fig. 1); however, the equilibrium is reached faster (i.e., 20 min). Another significant difference can be identified in the first stage of the sorption (insert in the figure). For sorption at pH 4, the relative concentration sharply decreases (almost linearly) during this initial stage (0–40 min); contrary to the kinetic profile at pH 8, where the sorption proceeds more slowly till 20 min (with parabolic shape).

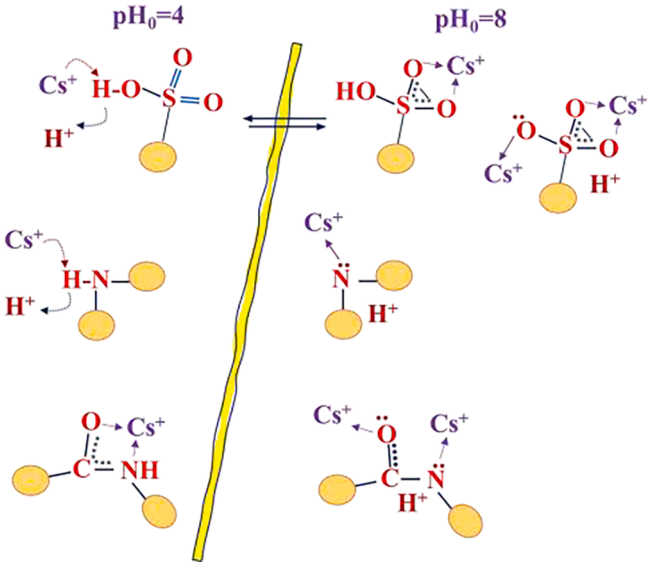

Scheme 2. Tentative sorption mechanisms for U(VI) binding onto ACES-F.

The kinetic profiles have been modeled using three conventional equations: (a) the pseudo-first (PFORE) and pseudo-second (PSORE) order rate equations (derived from chemical rate equations in homogeneous systems), and (b) the Crank equation (for resistance to intraparticle diffusion, RIDE) (See Table 1). These equations have been tested and the parameters (associated with the determination coefficient, i.e., R^2, and the Akaike Information Criterion, AIC) are summarized in Table 1. The quality of fitting for both pH 4 and pH 8, can be ranked according: PFORE > PSORE > RIDE. Main discrepancies between experimental profile and simulated curves are observed in the curved regions (20–40 min for pH 4 and 20–90 min for pH 8). It is noteworthy that the unexpected shape of the kinetic profile in the early stage at pH 8 leads to much lower correlation with the models. The calculated sorption capacities with the PFORE are closer to the experimental values (overestimation by 3–8 %) (compared with PSORE, overestimation by 17–32 %); as a confirmation that PFORE is more appropriate than PSORE for fitting uptake kinetics. Consistently with previous data increasing the pH increases sorption capacity from 0.619 ± 0.015 to 1.04 ± 0.010 mmol Cs g^{-1}). The apparent rate coefficient (k_1) is more than halved when the pH increases from pH 4 to pH 8: from 8.84 ± 0.32 × 10^{-2} to 3.93 ± 0.03 × 10^{-2} min^{-1}. In the case of hydroxysulfate green rust-modified aluminosilicate composite Huang et al. [47] did not report significant variation in the apparent rate coefficient between pH 2 and 12 (i.e., 5.6–5.8 × 10^{-2} min^{-1}).

The apparent rate coefficients are of the same order of magnitude than those reported for HNO_3-treated sawdust [48], metal organic framework (MOF = Nd-benzene tricarboxylic acid) [49] but higher than the values (2.0–5.8 × 10^{-3} min^{-1}) cited by Bezhin et al. [6] for a series of sorbents and ion-exchangers and by Erenturk et al. [32] for amino

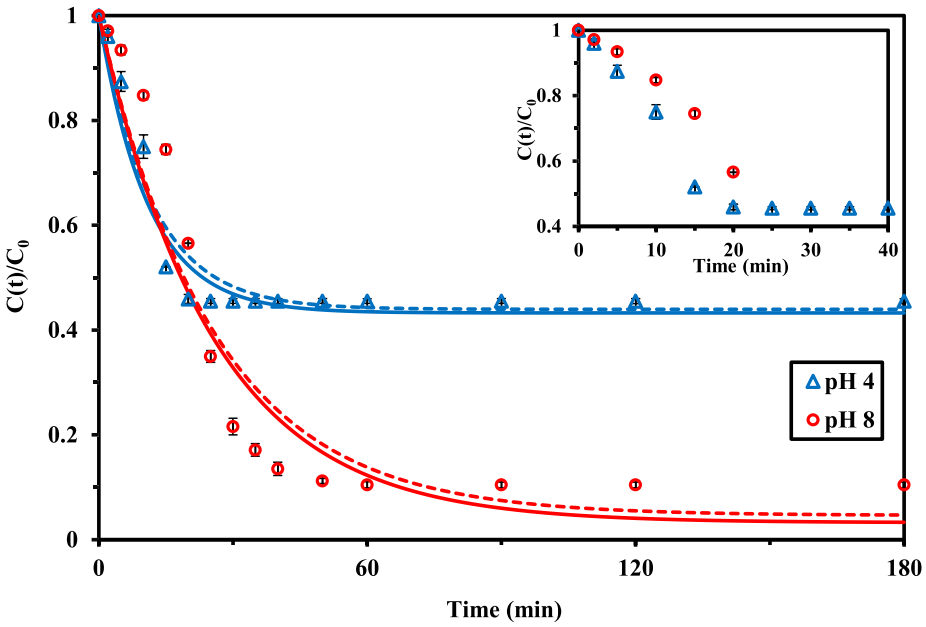

Fig. 2. Cs(I) uptake kinetics using ACES-F at pH 4 and pH 8 (C_0: 0.765 ± 0.015 mmol Cs L^{-1}; SD: 0.67 g/L; T: 20 ± 1 °C; time: 48 h; v: 210 rpm; average (+/- standard deviation) duplicated series: #1 and #2; fitted curves for Series #1 and #2 using the PFORE; insert: initial section).

Table 1
Cs(I) uptake kinetics using ACES-F sorbent – Parameters of PFORE, PSORE, and RIDE models.

pH		pH 4		pH 8	
Model	Parameter	#1	#2	#1	#2
Experim.	q_{eq}	0.634	0.604	1.03	1.05
PFORE	$q_{eq,1}$	0.655	0.623	1.11	1.13
	$k_1 \times 10^2$	9.16	8.52	3.95	3.90
	R^2	0.966	0.950	0.939	0.945
	AIC	−93	−87	−66	−69
PSORE	$q_{eq,2}$	0.738	0.711	1.36	1.38
	$k_2 \times 10^2$	16.3	15.3	2.97	2.89
	R^2	0.916	0.898	0.899	0.906
	AIC	−82	−79	−61	−63
RIDE	$D_e \times 10^{11}$	1.16	1.10	0.140	0.150
	R^2	0.927	0.909	0.882	0.890
	AIC	−81	−78	−55	−57

Units: q, mmol/L; k_1, min^{-1}; k_2, g $mmol^{-1}$ min^{-1}; D_e, m^2 min^{-1}.

pyridine sulfone amid resin (i.e., 7×10^{-3} min^{-1}). Faster kinetics were reported for metal-hexacyanoferate modified MOF (i.e., k_1: 0.1 min^{-1}) [50].

Despite weaker correlation between simulated and experimental values, the RIDE allows roughly evaluating the order of magnitude of the diffusion coefficient of Cs(I) in the sorbent. The effective diffusivity is significantly reduced while increasing the pH from 4 to 8 (consistently with the profiles) from $1.13 \pm 0.03 \times 10^{-11}$ to $0.145 \pm 0.005 \times 10^{-11}$ m^2 min^{-1}. These values are 4 to 5 orders of magnitude lower than the self-diffusivity of Cs(I) in water (i.e., 1.26×10^{-7} m^2 min^{-1}, [51]). This is indicative that the resistance to intraparticle diffusion contributes to the global control of uptake kinetics. In the case of Cs(I) sorption on Eu-AV-20 (microporous lanthanide silicate), Figuereido et al. [52] reported even lower diffusivities (by two orders of magnitude). The diffusivity of Cs(I) in extractant impregnated resin is slightly higher (i.e., 2.8×10^{-10} m^2 min^{-1}, [53]). The poor fitting of experimental profile with the Crank equation (especially at pH 8) means that other mechanisms are probably involved in the control of kinetics (associated with resistance to film diffusion, in complement to the reaction rate approached with the PFORE).

3.2.3. *Sorption isotherms and thermodynamics*

The sorption isotherms are reported in Fig. 3 for increasing temperatures (from 20 to 50 °C) at pH 4 and 8. Good reproducibility in sorption performances is confirmed by the low values of standard deviations. The profiles are characterized by a steep initial slope and the appearance of a saturation for residual Cs(I) concentrations close to 3 mmol Cs L^{-1}. This asymptotic trend allows anticipating that the Freundlich (power-type function) is not appropriate for fitting the distribution of the solute between solid (q_{eq}) and the liquid (C_{eq}) phases. Consistently with previous observations, the increase in temperature progressively decreases the sorption performance, as shown by both the sorption capacity at saturation (asymptotic values) and the initial slope of the curves (correlated with the affinity of the sorbent for the solute): the sorption is exothermic. The figure also confirms that increasing the pH significantly improves cesium binding. The sorption isotherms have been fitted with Langmuir, Freundlich, Sips and Temkin equations: Tables 2 and 3 summarize the parameters of these models for pH 4 and pH 8 data, respectively (calculations made on combined duplicated series; calculations on individualized series are reported in Tables S5 and S6). The isotherms are well fitted by Langmuir and Sips equations: statistical criteria are globally comparable and much better than with Temkin and Freundlich equations. The Langmuir equation supposes the sorption to occur as a monolayer without interactions between sorbed molecules; in addition, the distribution of sorption energies is homogeneous at the surface of the sorbent. The Sips equation is actually a combination of Langmuir and Freundlich equations; this equation counts on a three-adjustable parameters, which make the mathematical fit frequently better than the Langmuir equation (two-adjustable parameters), with a loss of physicochemical significance. Actually, here Langmuir is privileged for its physicochemical dimension: in Fig. 3, the solid lines represent the Langmuir fits (with the parameters reported in Tables 2 and 3) except for pH 8 and T: 20 °C where the Sips equation allows significantly improving the quality of the fit.

For pH 4 experiments, the maximum experimental capacity decreases from 1.46 to 0.99 mmol Cs g^{-1} (i.e., loss close to 33 %); consistently with the calculated maximum sorption capacity at saturation of the monolayer ($q_{m,L}$) that slightly overestimates experimental value, from 1.59 to 1.12 mmol Cs g^{-1}. The affinity coefficient (i.e., b_L) globally decreases with temperature (from 2.95 to 1.78 L $mmol^{-1}$). The impact of temperature is more marked at pH 8: the maximum sorption

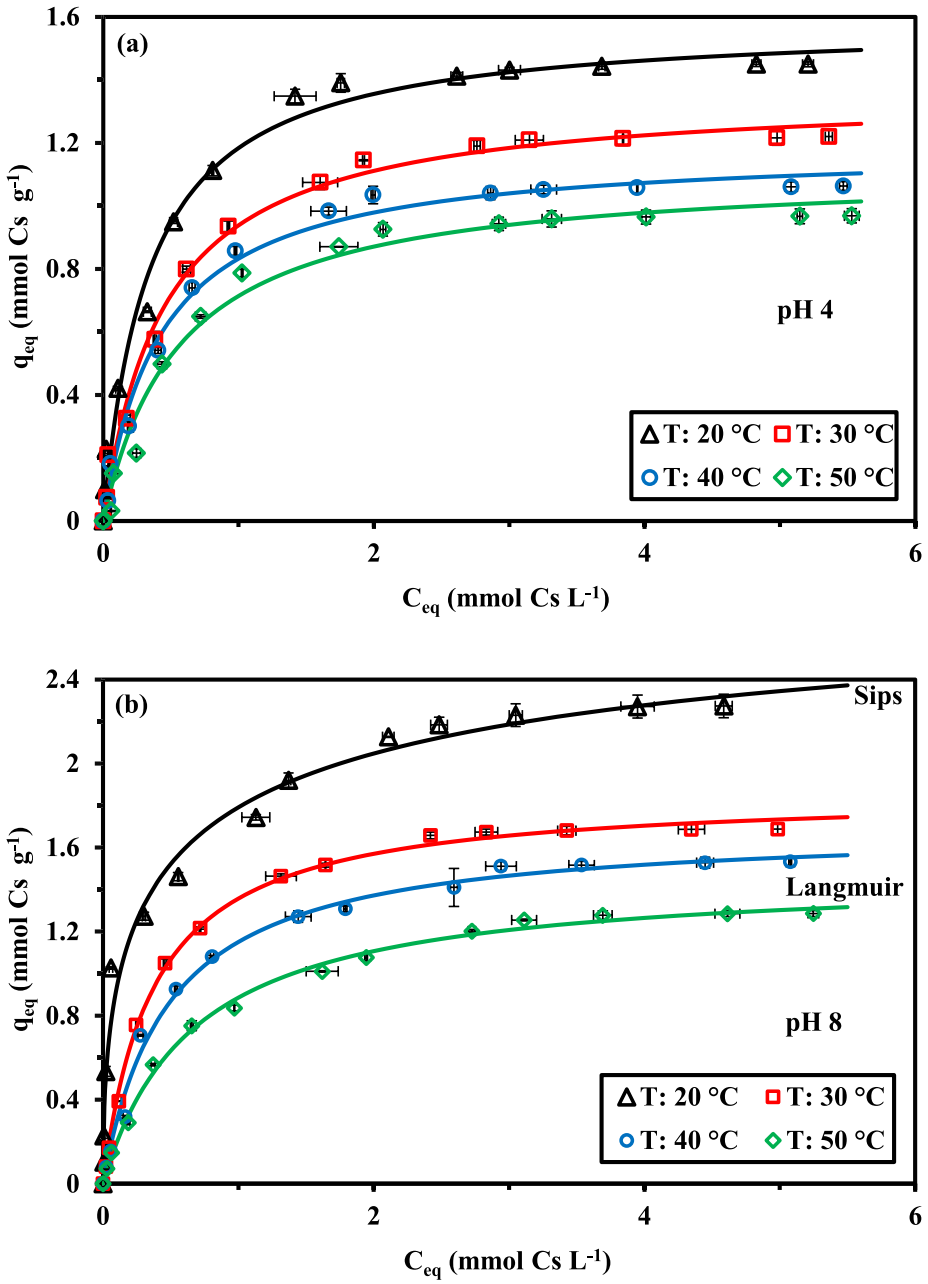

Fig. 3. Cs(I) sorption isotherms at pH 4 (a) and pH 8 (b) using ACES-F for increasing temperatures in the range 20–50 °C (C_0: 0.06–3.9 mmol Cs L^{-1}; pH_0: 4 → pH_{eq}: 3.8–4.2; pH_0: 8 → pH_{eq}: 5.9–6.4; v: 210 rpm; time: 48 h; average (+/- standard deviation) on duplicated series; fitted curves using the Langmuir equation, excepted at pH 4 and T: 20 °C with Sips equation).

capacity (i.e., $q_{m,exp}$) decreases by 44 % from 2.33 to 1.30 mmol Cs g^{-1} while the affinity coefficient is divided by ≈5 (from 7.64 to 1.50 L $mmol^{-1}$). The greater effect of temperature may be associated with a higher sensitivity of amine groups (which are responsible of the complementary binding occurring at this pH) to temperature for cesium binding. The percentage of increase in sorption capacity at pH 8 (compared with pH 4) represents 36.2 ± 1.2 %, 27.7 ± 2.3 %, 30.6 ± 0.1 %, and 24.7 ± 0.9 % at T: 20, 30, 40, and 50 °C, respectively. At pH 4 and T: 20 °C, the maximum sorption capacity reaches 1.46 mmol Cs g^{-1}, which is close to sulfonate content in ACES-F (elemental analysis: 1.55 mmol S g^{-1}); meaning that at saturation the stoichiometric ratio is close to 1:1 (i.e., 0.942:1), corresponding to the theoretical charge ratio between Cs^+ and $R\text{-}SO_3^-$). With the increase of the temperature, the deactivation of some of these reactive groups (endothermic sorption) decreases the stoichiometric ratio to lower values (≈0.64:1). At pH 8 and 20 °C, the sorption capacity reaches 2.33 mmol Cs g^{-1}; meaning a difference of 0.776 mmol Cs g^{-1} (compared with pH 4). This additional sorption may be associated with amine groups (≈5.60 mmol N g^{-1}). The additional cesium binding is much lower than the amount of amine groups; this may be explained by steric hindrance and/or the co-existence of different *N*-based groups that have different affinity and reactivity with Cs(I) (depending on their chemical environment in the sorbent).

The affinity coefficients of the Langmuir equation (i.e., b_L) and the van't Hoff equation were used for calculating thermodynamic parameters, according Tran et al., [54]):

$$\Delta G^{\circ} = \Delta H^{\circ} - T\Delta S^{\circ} \quad (1a)$$

$$\ln b_L^{*} = \frac{-\Delta H^{\circ}}{R} \times \frac{1}{T} + \frac{\Delta S^{\circ}}{R} \quad (1b)$$

Table 2
Cs(I) sorption isotherms at pH 4 using ACES-F – Parameters of Langmuir, Freundlich, Sips and Temkin models (parameters determined from combined Series #1 and #2).

		Temperature (±1° C)			
Model	Parameter	20	30	40	50
Experimental	$q_{m,exp.}$	1.46	1.24	1.08	0.991
Langmuir	$q_{eq,L}$	1.59	1.36	1.19	1.12
	b_L	2.95	2.21	2.35	1.78
	R^2	0.988	0.989	0.989	0.983
	AIC	−146	−161	−171	−160
Freundlich	k_F	1.03	0.818	0.720	0.621
	n_F	3.58	3.24	3.30	2.97
	R^2	0.931	0.929	0.908	0.899
	AIC	−102	−111	−111	−113
Sips	$q_{eq,S}$	1.63	1.35	1.13	1.00
	b_S	2.55	2.30	3.04	3.10
	n_S	1.10	0.972	0.839	0.670
	R^2	0.987	0.989	0.992	0.991
	AIC	−144	−159	−174	−165
Temkin	A_T	96.7	48.2	38.6	22.5
	b_T	9.91	10.8	12.1	12.3
	R^2	0.963	0.968	0.967	0.657
	AIC	−120	−134	−140	−137

Units: q, mmol g^{-1}; b, L $mmol^{-1}$; n, dimensionless; k_F, $mmol^{1-1/nF}$ $L^{-1/nF}$ g^{-1}; A_T, L $mmol^{-1}$; b_T, J kg mol^{-2}.

Table 3
Cs(I) sorption isotherms at pH 8 using ACES-F – Parameters of Langmuir, Freundlich, Sips and Temkin models (parameters determined from combined Series #1 and #2).

		Temperature (±1° C)			
Model	Parameter	20	30	40	50
Experimental	$q_{m,exp.}$	2.33	1.71	1.56	1.30
Langmuir	$q_{eq,L}$	3.19	1.86	1.70	1.48
	b_L	7.64	2.68	2.09	1.50
	R^2	0.946	0.997	0.990	0.992
	AIC	−83	−177	−153	−155
Freundlich	k_F	1.66	1.16	0.989	0.781
	n_F	3.81	3.16	2.94	2.72
	R^2	0.964	0.926	0.934	0.950
	AIC	−96	−91	−100	−117
Sips	$q_{eq,S}$	3.12	1.81	1.64	1.52
	b_S	1.35	3.23	2.46	1.38
	n_S	1.99	0.902	0.911	1.06
	R^2	0.981	0.998	0.991	0.992
	AIC	−111	−183	−152	−154
Temkin	A_T	261	44.8	35.3	29.3
	b_T	7.51	7.51	8.41	10.2
	R^2	0.986	0.980	0.974	0.978
	AIC	−122	−128	−127	−141

Units: q, mmol g^{-1}; b, L $mmol^{-1}$; n, dimensionless; k_F, $mmol^{1-1/nF}$ $L^{-1/nF}$ g^{-1}; A_T, L $mmol^{-1}$; b_T, J kg mol^{-2}.

$$b_L^* = b_L \times \frac{C^0_{sorbate}}{\gamma_{sorbate}} (\text{with } b_L \text{ in L mol}^{-1}) \quad (1c)$$

ΔG° (kJ mol^{-1}), Gibbs free energy change; ΔH° (kJ mol^{-1}), enthalpy change; ΔS° (J mol^{-1} K^{-1}), entropy change; R (8.314 J mol^{-1} K^{-1}), universal gas constant; T (K), absolute temperature; $C^\circ_{sorbate}$: ≈1 mol L^{-1}, unitary standard concentration of the sorbate; $\gamma_{sorbate}$: ≈1 for dilute solutions, activity coefficient.

Table 4 reports the values of the thermodynamic parameters for Cs(I) sorption at pH 4 and pH 8. The negative value of the enthalpy change confirms the exothermic nature of cesium sorption; metal binding becomes more exothermic as the pH increases. It is noteworthy that the entropy change shows remarkable differences between pH 4 and pH 8: positive in acidic solutions, it becomes negative in alkaline solutions. The entropy change is associated with the order/disorder of the system:

Table 4
Thermodynamic parameters for Cs(I) sorption using ACES-F – Application of van't Hoff equation.

	pH 4			pH 8		
T (K)	ΔH°	ΔS°	ΔG°	ΔH°	ΔS°	ΔG°
293	−11.50	26.92	−19.38	−30.78	− 34.76	−20.60
303			−19.65			−20.25
313			−19.92			−19.90
323			−20.19			−19.56
R^2	0.822				0.931	
	$\lvert\Delta G^\circ\rvert > \lvert T \times \Delta S^\circ\rvert$			$\lvert\Delta G^\circ\rvert > \lvert T \times \Delta S^\circ\rvert$		

Units: ΔH° and ΔG°, kJ mol^{-1}; ΔS°, J mol^{-1} K^{-1}.

herein, the order in the system increases with the pH due to higher binding efficiency (cesium chelation on amine groups, despite greater pH variation associated with proton release). The Gibbs free energy hardly changes with temperature and pH remaining close to -20 ± 1 kJ mol^{-1}. The sorption is controlled by enthalpy rather than by entropy since $|\Delta G^\circ|$ is systematically higher than $|T \times \Delta S^\circ|$. The comparison of thermodynamic parameters for Cs(I) sorption with the values reported for alternative sorbents (Table S7) does not allow correlating specificities (endo/exothermic nature of sorption, signs of changes in entropy and Gibbs free energy) to specific pH or binding mechanism.

The Cs(I) sorption performances of ACES-F are compared with literature in Table S4. At pH 8, the maximum sorption capacity ($q_{m,\ exp.}$: 2.22 mmol Cs g^{-1}) is among the most efficient sorbents, similar to functionalized zeolite (nano 2-naphtyl amine 6:6-azulene sodium methanesulfonate disulfonic acid-impregnated zeolite, 1.96 mmol Cs g^{-1}, [55]) and metal hexacyanoferrate/PVA hydrogel (1.51 mmol Cs g^{-1}, [56]). Their relevant affinity coefficients (i.e., b_L) are of the same order of magnitude (1.54–2.32 L $mmol^{-1}$). It is noteworthy that the kinetic parameter (equilibrium time) is much more favorable for ACES-F and functionalized zeolite (i.e., 40–60 min), compared with metal hexacyanoferrate/PVA hydrogel (i.e., 1440 min). Considering acidic solutions (pH 4–5), ACES-F is also highly efficient ($q_{m,exp}$ and b_L parameters) for Cs(I) removal compared with alternative materials. Globally, ACES-F shows remarkable sorption properties both in terms of maximum sorption capacity, affinity coefficient and pH adaptability.

3.2.4. *Selectivity issues*

The other challenges in the design of sorbents that are targeted to remove metal ions in solutions as complex as brines and/or seawater concern the selective sorption properties, which may concern both competitor metal ions or counter anions in considerably higher concentrations.

3.2.4.1. Effect of ionic strength – NaCl addition. The effect of NaCl addition on Cs(I) sorption is tested at different pH_{eq} values (Fig. S11). As expected, the sorption capacity continuously increases with the pH, whatever the concentration of the salt. The introduction of increasing amounts of NaCl systematically reduces the sorption capacity. However, even with a huge excess of salt (i.e., 4 M *vs* 1.08 mmol Cs L^{-1}) the sorption remains highly efficient: at pH_{eq} ≈4, the sorption capacity decreases from 0.60 to 0.28 mmol Cs g^{-1} (from 1.09 to 0.49 mmol Cs g^{-1} at pH 8.6). Recently, Bezhin et al. [6] compiled the maximum sorption capacities of a series of sorbents for Cs(I) recovery from seawater (i.e., with lower NaCl concentration, i.e., ≈0.24–0.27 mmol Na L^{-1}; but with presence of other competitor ions): the sorption capacities ranged between 0.014 and 0.13 mmol Cs g^{-1}. In the current test, the maximum sorption capacity is not determined (experimental series with a single fixed C_0 value; 1.08 mmol Cs L^{-1}, which does not correspond to the saturation concentration in the isotherms). This means that ACES-F maintains remarkable sorption capacity even in the presence of huge excess of NaCl. In the case of ion-exchange mechanism, the ionic strength and presence of large excess of other ions may strongly affect

the binding of metal ions due to competitor and shielding effects. These results confirm that cesium binding onto ACES-F proceeds through complementary mechanisms such as chelation. Fig. S11 also shows that the typical two-waves shape of the curve observed without NaCl (with local optima at pH 4 and 8) is progressively smoothed when NaCl concentration increases. This is typically illustrated by the largest decreases observed in sorption capacities in the regions pH 2–3 and pH 7–8: these regions correspond to local optimum pH values reported in section 3.2.1., associated with different modes of interaction (and protonation of reactive groups).

3.2.4.2. Effect of competitor cations. The selectivity of ACES-F sorbent against other metal ions was investigated through the study of Cs(I) recovery from multicomponent solutions (containing Na(I), Ca(II), Mg (II), Fe(III), Al(III), Sr(II)). These metal ions have been selected as representative of common mono-, di- and tri-valent elements, with similar initial concentrations (0.54 mmol Ca L^{-1} and 0.83–1.08 mmol L^{-1} for other metal ions); the initial pH_0 was varied between 3.3 and 8.02 (pH_{eq}: 3.18–6.98). The selectivity coefficient ($SC_{Cs/metal}$, dimensionless) for Cs against other metal ions was defined as:

$$SC_{Cs/metal} = \frac{D_{Cs}}{D_{metal}} = \frac{q_{eq,Cs} \times C_{eq,metal}}{C_{eq,Cs} \times q_{eq,metal}} \quad (2)$$

Fig. 4 compares the $SC_{Cs/metal}$ values for different values of pH_{eq}. The highest selectivity of ACES-F for Cs(I) is reached at pH_{eq} 6.31 (i.e., pH_0: 7.02). In addition, the SC values can be ranked according:

Na(I) (97.1) ≫ Mg(II) (32.6) > Ca(II) (30.0) > Al(III) (25.8) ≫ Fe(III) (10.6) ≫ Sr(II) (5.1).

ACES-F shows an outstanding preference for Cs(I) against Na(I); this is remarkably promising for the treatment of seawater. For divalent alkali cations (i.e., calcium and magnesium), the SC values are much lower but the sorbent keeps a large preference for Cs(I) (SC higher than 32). It is noteworthy that the selectivity against Sr(II) (also ranked among alkali metal ions) sharply drops to 5.1: meaning that the ionic charge is not the predominant parameter. Fig. S12 shows the SC values for Sr(II) against other competitor metals; the figure shows that ACES-F has also a marked preference for Sr(II) than for other competitor metals (except cesium). In the case of trivalent cations, the selectivity coefficient differentially decreases: relatively close to divalent alkali metal cations for Al(III) (around 26) while it sharply decreases for Fe(III) (down to 11). Other parameters such as ionic radius, configuration could influence this selectivity. For example, Cs(I) is distinguished by a 12-coordinated configuration (with large ionic radius, r: 1.70 Å) [57]. Other metal ions are characterized by: (a) octahedron structure, such as Na(I) (r: 1.02 Å), Mg(II) (r: 0.72 Å), Al(III) (r: 0.53 Å), or Fe(III) (r: 0.65 Å), or (b) square-antiprism configuration, such as Ca(II) (r: 1.00 Å), and Sr(II) (r: 1.25 Å). It is not possible directly and simply correlating the differences in selectivity coefficients among each metal classes (mono-, di-, and trivalent) with the configuration nor the R_p value. Fig. S13 shows the distribution maps of the SC values and the distribution ratios of individual metals with two indices: (i) the ionic index (i.e., z^2 / r), and (ii) the covalent index (i.e., $X_m^2 \times r$), where z is the ionic charge, and X_m is the Pauling electronegativity. In this figure, the metals are grouped by similar ionic charge. In each ionic charge group, the distribution ratio D is favored by high ionic radii, while the SC values follow a reciprocal trend. It is noteworthy that the amplitudes decrease according mono- ≫ di- > trivalent groups and that the Ionic Index allows better "segregating" the groups (avoiding superposition, as it may occur with the covalent index). At pH 7, sulfonate groups are directly and totally involved in metal sorption, while a fraction of amine groups may also contribute. All these metal ions are classified as Hard acids according Pearson' rules [58], meaning that they have high affinity for Hard bases bearing O- and N- donor atoms (such as sulfonate > amine functional groups).

3.2.5. Cesium desorption and sorbent recycling

Cesium is successfully desorbed using acidic solution (i.e., 0.3 M HNO_3 solution). The acidic solution (pH ≈ 0.5) reverses the sorption by protonation of amine groups (for sorbent loaded at pH 8) and/or competition effect of nitrate ions (ion-exchange of Cs(I) from sulfonate groups at pH 4 and 8). This is consistent with the negligible sorption observed at pH 1 (Fig. 1). Milyutin et al. [59] also used nitric acid solutions (0.5–1 M) for complete desorption of Cs(I) from resorcinol-formaldehyde sorbents. Nitric acid solutions were much less efficient for the elution of Cs(I) bound onto metal hexacyanoferrate deposited on MOF (i.e., only around 25 %, [50]). Potassium chloride (2 M) was also reported for the desorption (yield close to 92 %) of Cs(I) from Cu-HCF/anthranilic acid-aminophenol copolymer [60]. In the case of *Punica granatum* peel (pomegranate-based sorbent) alkaline solutions (0.5 M NaOH) revealed slightly more efficient than 0.1 M and 0.5 M HNO_3

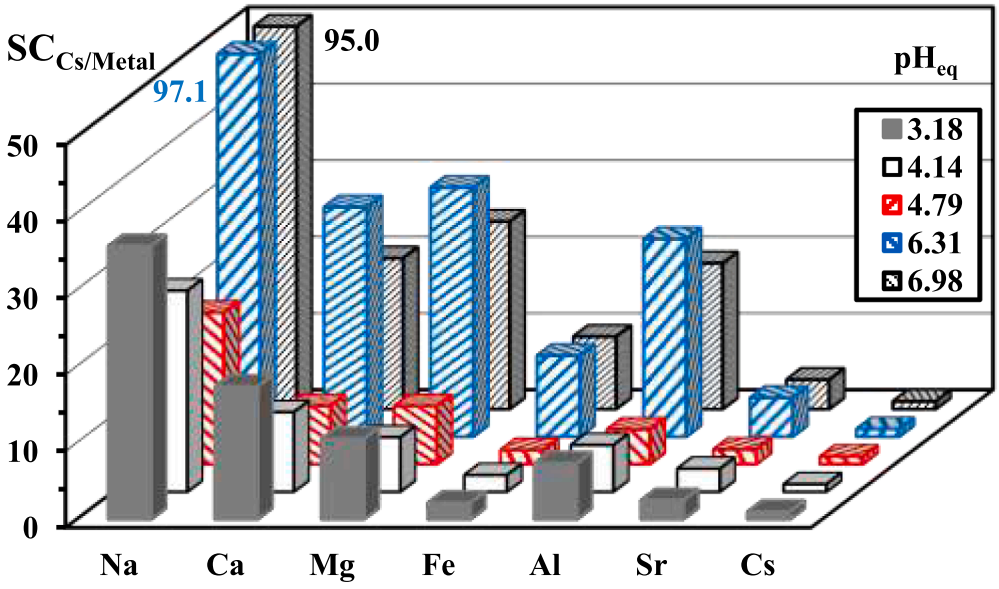

Fig. 4. Influence of pH on the separation of Cs(I) from other metal ions in multicomponent solutions using ACES-F (C_0: 0.934 mmol Na L^{-1}; 0.542 mmol Ca L^{-1}; 1.01 mmol Mg L^{-1}; 0.834 mmol Fe L^{-1}; 0.857 mmol Al L^{-1}; 0.949 mmol Sr L^{-1}; 1.077 mmol Cs L^{-1}; SD: 1.6 g L^{-1}; T: 20 ± 1 °C; v: 210 rpm; time: 24 h; $SC_{Cs/Cs} = 1$, as reference).

solutions [61]. Thirty minutes of contact are sufficient for achieving the complete release of Cs(I) (under selected experimental conditions) (Fig. S14). The profiles are superposed for sorbent loaded at both pH 4 and pH 8 within the first 10 min of contact; above, cesium desorption is slightly more efficient and faster at pH 8 (total desorption occurs at time: 25 min). This is the reciprocal trend to that observed for uptake kinetics, where the sorption at pH 8 was slightly lower than at pH 4.

A rinsing step (using demineralized water) was systematically applied (between each sorption and desorption steps) for the study of sorbent recycling. Table 5 compares the sorption and desorption efficiencies for five successive cycles. The desorption efficiency was systematically complete (>99.8 %). The sorption efficiencies slightly decrease with recycling; however, the loss in sorption performance remains very limited (about 1.3 % and 2.1 % at pH 4 and 8, respectively). Amin et al. [50] reported a 9 % loss in sorption efficiency for Metal-HCNF/MOF sorbent. For Prussian blue loaded onto *N*-doped porous carbon, Li et al. [62] reported that the loss in cesium sorption may reach up to 13 % at the fifth cycle. The loss in Cs(I) sorption reached 8.5 % at the fifth cycle in the case of phosphomolybdic acid/PCN-224 composite [63]. The sorption and desorption performances are outstandingly stable while using ACES-F sorbent under selected experimental conditions; confirming the interest of this new sorbent for Cs(I) recovery.

3.3. Application to real effluent

Two seawater samples were collected from the coasts of Ra's Gharib (Red Sea, Egypt) and Da Nang (Vietnam) (Fig. S15). Table S8 reports the concentration of selected elements in these two samples. The molar ratio (referred to cesium) is also calculated to show the huge excess of competitor elements: the concentrations of major elements (Na, K, Mg, and Ca) are 5.4-to 555-folds the concentration of cesium, for competitor elements (Sr and B) the excess ranges between 25 and 344 times. Apart cesium, two trace elements are also considered (U and As, with molar ratio in the range 0.018–0.46). The sorption tests were performed at the natural pH (i.e., 7.46–7.51). Figs. S16 and S17 shows the uptake kinetics for selected metals using ACES-F in the treatment of seawater samples (at their natural pH values). The sorption is significantly longer than expected from uptake profiles reported for synthetic solutions. Herein, the equilibrium is reached after 24 h of contact (probably more for cesium, strontium, and arsenic). Logically, the huge excess of major elements causes their much higher sorption (2–20 mmol g^{-1}, compared with Cs and Sr, where the maximum sorption capacities do not exceed 0.12 mmol Sr g^{-1} and 2.2–4 μmol Cs g^{-1}. At equilibrium, the sorption capacities for Cs(I) reach 0.53 mg Cs g^{-1} (i.e., 3.99 μmol Cs g^{-1}) and 0.285 mg Cs g^{-1} (i.e., 2.14 μmol Cs g^{-1}) for Da Nang (Vietnam) and Ra's Gharib (Egypt) samples, respectively. These values are below the levels reported for maximum sorption capacities (in the range 0.014 and 0.13 mmol Cs g^{-1}) by Bezhin et al. [6]. The comparison is made difficult by different experimental conditions (including sorbent dose: herein 0.2 g L^{-1} *vs* 0.05 g L^{-1} for cited work). In addition, the sorption capacity is reported for discrete value and not as maximum sorption capacity (at saturation of the sorbent). Extensive studies (varying sorbent dose) would help for the comparison of sorption performances. However, Bezhin et al. [6] report the high sorption capacities of sorbents incorporating Prussian Blue analogues despite much higher sorbent dose (10 g L^{-1}); this can be explained by the exceptional selectivity of Prussian Blue for cesium [11].

Table S9 compares for selected elements the sorption efficiencies (%) and the distribution coefficients (L g^{-1}). Logically for major elements in large excess) the sorption efficiencies are below 6 % and their distribution coefficients remain below 0.34 L g^{-1}. On the opposite hand, for trace elements (including cesium) and competitor elements (i.e., Sr and B) the sorption efficiencies vary between 20 % and 55 %, with D values ranging between 1.24 and 6.12 L g^{-1}).

Sorption performances for seawater samples are influenced by the concentration of the elements; cesium (as strontium) is significantly enriched in the sorbent (D around 3 L g^{-1} for both Cs(I) and Sr(II); under selected experimental conditions, 36–39 % of the metal is recovered.

3.4. Antimicrobial activity and cytotoxic effect

The use of a sorbent for removing a metal is targeted to recover valuable resource and/or solving an environmental problem. In this context, it may be interesting evaluating its environmental impact when used in water bodies and living organisms (including humans). This may be also used for developing new active compounds. Several criteria may be used for quantifying these effects; herein, two criteria have been analyzed: (a) the antimicrobial activity of ACES-F onto the growth of two Gram-positive, two Gram-negative bacteria and one unicellular fungus, and (b) the toxicity of the sorbent for human cell lines (2 normal ones, and one carcinogenic). Section E in Supplementary Information provides a detailed information on the experimental procedures that were applied for this study, and an extensive discussion of experimental results. Herein, the main conclusions are summarized.

In Fig. 5, the antimicrobial effect of ACES-F is measured through the determination of the inhibition zone (well method) for different doses of the sorbent. The material is characterized by a wide spectrum of action. Indeed, all the microorganisms are inhibited by the presence of ACES-F. Obviously, for a dose of 100 μg L^{-1} or above, the effect is little more marked for Gram-negative microorganisms (*E. coli* and *P. aeruginosa*) than for Gram-positive bacteria (*B. subtilis*, *S. aureus*) and unicellular fungus (*C. albicans*). While the amount of polymer decreases to 50 μg L^{-1}, a weaker inhibition is maintained for *S.aureus*, *P. aeruginosa* and *E. coli*. At the dose of 25 μg L^{-1}, ACES-F shows a limited inhibition only for *P. aeruginosa*. Several hypotheses may be proposed for explaining these differential antimicrobial activities; characterized by MIC values (minimum inhibitory concentration) close to 25 μg L^{-1} for *P. aeruginosa*, 50 μg L^{-1} for *E. coli* and *S. aureus*, and up to 100 μg L^{-1} for *B. subtilis* and *C. albicans*. The inhibitory effect of ACES-F could be attributed to:

(a) the composition of the cell walls (Gram-positive bacteria hold a peptidoglycan external layer that limits the diffusion of active compounds, while anionic liposaccharide compounds in Gram-negative bacteria facilitate the accumulation of the active compounds),

Table 5
Sorbent recycling – Sorption efficiency (SE, %) and desorption efficiency (DE, %) for five successive cycles using ACES-F (loaded at pH 4 and pH 8).

pH	4				8			
Cycle	SE (%)		DE (%)		SE (%)		DE (%)	
	Aver.	St. dev.	Aver.	St. dev.	Aver.	St. dev.	Aver.	St. dev.
#1	54.1	0.4	99.9	0.2	98.8	0.1	100.0	0.0
#2	53.5	0.0	99.9	0.2	98.0	0.1	100.0	0.1
#3	52.9	0.2	100.0	0.1	97.8	0.0	100.0	0.0
#4	52.6	0.0	100.0	0.0	97.0	0.1	100.1	0.0
#5	52.4	0.0	100.1	0.1	96.7	0.1	99.9	0.2
Loss (5th/1st)	1.3 %				2.1 %			

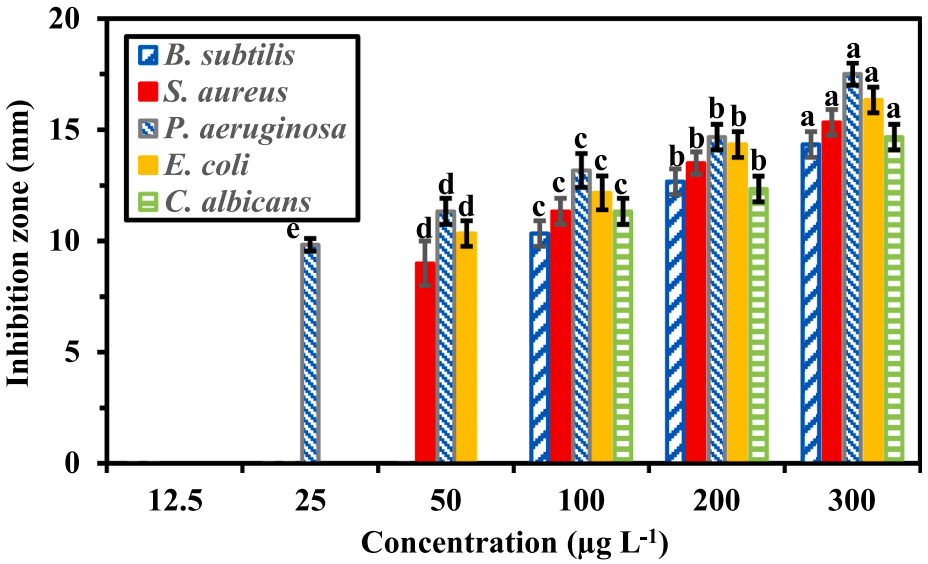

Fig. 5. Antimicrobial effect of sorbent against pathogenic Gram-positive (*B. subtilis* and *S. aureus*), Gram-negative bacteria (*E. coli* and *P. aeruginosa*), and unicellular fungi (*C. albicans)*. The results shows the averaged value of the zone of inhibition (mm) for three replicates (with ± SD). For a given microorganism, different letters on the bars identify statistically representative differences in the ZOI (with $p \leq 0.05$), while increasing the concentration.

(b) the penetration of reactive oxygen species and toxic free radicals (provoking cell death),
(c) the action of the reactive groups of ACES (the precursor) (destruction of sterol-based compounds, due to interferences with the synthesis pathway of ergosterol; in the case of yeast).

The cytotoxicity of ACES-F was tested (with different concentrations) against three cell lines: HFB4 and Vero cells (normal cell lines) and caco-2 cells (carcinogenic cell line). The MTT method is a sensitive colorimetric method involving 3-[4,5-dimethylthiazole-2-yl]-2,5-diphenyltetrazolium bromide, which is used for quantifying the numeration of living cells. Fig. S18 shows morphological changes such as shrinking, roundness, and granulation effect increasing with concentration (phase-contract microscopy). In addition, some damages to the epithelial layer may be observed. Complementary MTT assays helped quantifying the cell viability in function ACES-F concentration (Fig. 6). The IC_{50} parameter (concentration for 50 % cell mortality) for normal cell lines is 12- to 15-fold the value obtained for carcinogenic cell line: 284.4 ± 11.8 µg mL^{-1} and 361.1 ± 11.5 µg mL^{-1} for Vero and HFB4, respectively, against 24.3 ± 12.8 µg mL^{-1} for Caco-2. These data confirm that at low ACES-F concentration, the material shows an anti-proliferative impact on cancer cell line (contrary to normal cells). Therefore, these preliminary results open a therapeutic window for applying ACES-F as a chemotherapeutic agent. On the other hand, the material requires much higher concentration for significantly affecting the viability of normal cell lines (i.e., Vero and HFB4). This also means that ACES-F can be used in water treatment even at concentration as high as 1000 µg mL^{-1} without causing harmful effects to normal human cells.

Based on biological tests, it can be concluded that, besides the promising reactivity of synthesized polymer for cesium removal, ACES-F can be used for treatment the contaminant water containing different pathogens. This polymer can be applied with high concentrations

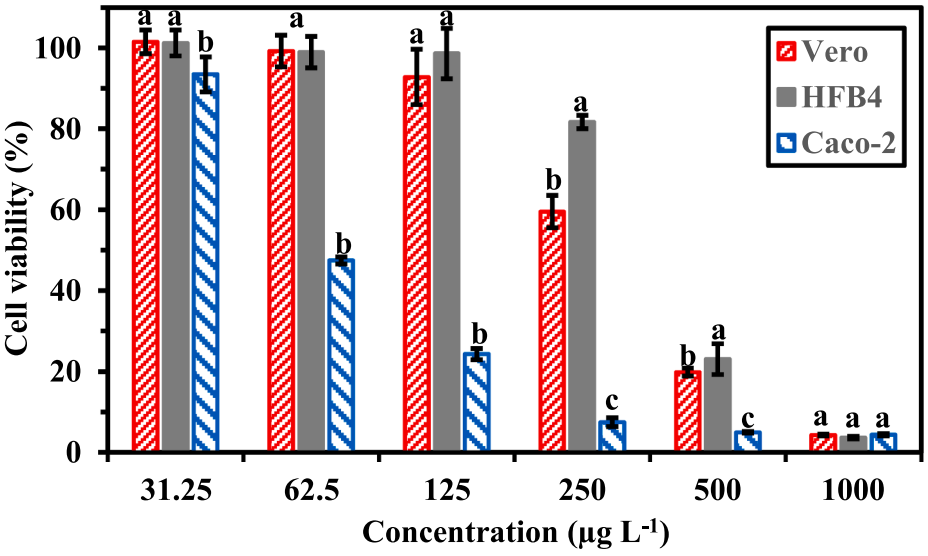

Fig. 6. Cell viability of normal cell lines (Vero and HFB4) and cancer cell lines (Caco-2) in contact with the sorbent at different concentrations and assessed using the MTT assay method (data are represented as averaged value and standard deviation for 3 replicates; for a given concentration, different letters indicates statistically different responses in the viability of target cell).

without any impact on normal mammalian cells, while the polymer is reactive against cancerous cells.

4. Conclusion

The thorough study of Cs(I) sorption properties shows that the simple one-pot synthesis of ACES-F (obtained by reaction of formaldehyde with N-(2-acetamido)-2-aminoethanesulfonic acid) offers promising perspectives for the recovery of cesium from complex effluents (including seawater, as a premise for future work on the treatment of samples contaminated with radioelements). This is confirmed by the relatively weak effect of ionic strength (varied by increasing additions of NaCl) and competitor ions. Amine and sulfonic groups contribute to the high sorption and selectivity. The simple procedure produces a stable sorbent in terms of recycling properties (negligible loss in sorption and desorption after five cycles), with one of the highest sorption capacity compared with literature data (i.e., maximum sorption capacity close to 2 mmol Cs g^{-1}). Fast kinetics for both sorption and desorption can be correlated with the mesoporous structure of sorbent microparticles.

In order to evaluate the harmlessness in the use of the sorbent, MTT tests were successfully carried out for checking the cytotoxity of the sorbent (and critical concentration) on the viability of normal cells. Surprisingly, ACES-F has very limited cytotoxicity for these normal cells while it reveals highly effective for inhibiting the development of cancerous cells. On the other hand, the sorbent develops antimicrobial properties against Gram+, Gram- and pathogenic yeast.

Declaration of Competing Interest

The authors declare that they have no known competing financial interests or personal relationships that could have appeared to influence the work reported in this paper.

Data availability

Data will be made available on request.

Acknowledgements

Yuezhou WEI acknowledges the National Natural Science Foundation of China for supporting the projects U1967218 and 11975082.

Appendix A. Supplementary data

Supplementary data to this article can be found online at https://doi.org/10.1016/j.cej.2022.140155.

References

[1] D. Alby, C. Charnay, M. Heran, B. Prelot, J. Zajac, Recent developments in nanostructured inorganic materials for sorption of cesium and strontium: synthesis and shaping, sorption capacity, mechanisms, and selectivity-a review, J. Hazard. Mater. 344 (2018) 511–530.
[2] K. Patra, A. Sengupta, R.K. Mishra, V.K. Mittal, T.P. Valsala, C.P. Kaushik, Assessing the feasibility study of highly efficient and selective co-sequestration process for cesium and strontium utilizing calix-crown and crown-ether based combined solvent systems, J. Radioanal. Nucl. Chem. 331 (2022) 1473–1481.
[3] K. Patra, B. Sadhu, A. Sengupta, C.B. Patil, R.K. Mishra, C.P. Kaushik, Achieving highly efficient and selective cesium extraction using 1,3-di-octyloxycalix 4 arene-crown-6 in n-octanol based solvent system: experimental and DFT investigation, RSC Adv. 11 (35) (2021) 21323–21331.
[4] R.B. Gujar, S.A. Ansari, W. Verboom, P.K. Mohapatra, Multi-podant diglycolamides and room temperature ionic liquid impregnated resins: an excellent combination for extraction chromatography of actinides, J. Chromatogr. A 1448 (2016) 58–66.
[5] O.A. Abdel Moamen, H.S. Hassan, W.F. Zaher, Taguchi L16 optimization approach for simultaneous removal of Cs^{+} and Sr^{2+} ions by a novel scavenger, Ecotoxicol. Environ. Saf. 189 (2019), 110013.
[6] N.A. Bezhin, I.I. Dovhyi, E.A. Tokar, I.G. Tananaev, Physical and chemical regularities of cesium and strontium recovery from the seawater by sorbents of various types, J. Radioanal. Nucl. Chem. 330 (2021) 1101–1111.
[7] T. Abdollahi, J. Towfighi, H. Rezaei-Vahidian, Sorption of cesium and strontium ions by natural zeolite and management of produced secondary waste, Environ. Technol. Innov. 17 (2020), 100592.
[8] O. Eljamal, T. Shubair, A. Tahara, Y. Sugihara, N. Matsunaga, Iron based nanoparticles-zeolite composites for the removal of cesium from aqueous solutions, J. Mol. Liq. 277 (2019) 613–623.
[9] D.R. Ferreira, G.D. Phillips, B. Baruah, A comparison of the adsorption of cesium on zeolite minerals vs. vermiculite, Clays Clay Miner. 69 (2021) 663–671.
[10] A.B. Ginting, A. Siti, Noviarty, Yanlinastuti, A. Nugroho, Boybul, Natural zeolite as a replacement for resin in the cation exchange process of cesium on post-irradiated nuclear fuel, Nukleonika 66 (2021) 11–19.
[11] C. Vincent, A. Hertz, T. Vincent, Y. Barre, E. Guibal, Immobilization of inorganic ion-exchanger into biopolymer foams - Application to cesium sorption, Chem. Eng. J. 236 (2014) 202–211.
[12] C. Vincent, Y. Barre, T. Vincent, J.M. Taulemesse, M. Robitzer, E. Guibal, Chitin-Prussian blue sponges for Cs(I) recovery: from synthesis to application in the treatment of accidental dumping of metal-bearing solutions, J. Hazard. Mater. 287 (2015) 171–179.
[13] Z. Li, Z. Zhang, J. Cheng, Q. Li, B. Xie, Y. Li, S. Yang, Stabilization of Prussian blue analogues using clay minerals for selective removal of cesium, J. Mol. Liq. 345 (2022) 117823.
[14] J. Huo, G. Yu, J. Wang, Selective adsorption of cesium (I) from water by Prussian blue analogues anchored on 3D reduced graphene oxide aerogel, Sci. Total Environ. 761 (2021), 143286.
[15] T.T. Li, F. He, Y.D. Dai, Prussian blue analog caged in chitosan surface-decorated carbon nanotubes for removal cesium and strontium, J. Radioanal. Nucl. Chem. 310 (2016) 1139–1145.
[16] S.-C. Jang, S.-M. Kang, Y. Haldorai, K. Giribabu, G.-W. Lee, Y.-C. Lee, M.S. Hyun, Y.-K. Han, C. Roh, Y.S. Huh, Synergistically strengthened 3D micro-scavenger cage adsorbent for selective removal of radioactive cesium, Sci. Rep. 6 (2016) 38384.
[17] P.-H. Wang, Y.-R. Chang, M.-L. Chen, Y.-K. Lo, D.-J. Lee, Shape stable poly(vinyl alcohol) hydrogels with immobilized metal hexacyanoferrates for cesium removal from waters, Environ. Sci. Pollut. Res. 29 (2022) 12427–12433.
[18] K. Patra, S.A. Ansari, P.K. Mohapatra, Metal-organic frameworks as superior porous adsorbents for radionuclide sequestration: current status and perspectives, J. Chromatogr. A 1655 (2021), 462491.
[19] B. Prelot, I. Ayed, F. Marchandeau, J. Zajac, On the real performance of cation exchange resins in wastewater treatment under conditions of cation competition: the case of heavy metal pollution, Environ. Sci. Pollut. Res. 21 (15) (2014) 9334–9343.
[20] R. Kumar, P. Malodia, M. Kachwaha, S. Verma, Adsorptive and kinetic studies of resin for removal of Cs^{+} and Sr^{2+} from aqueous solution, J. Water Chem. Technol. 41 (2019) 292–298.
[21] Y. Hu, X. Guo, C. Chen, J. Wang, Algal sorbent derived from *Sargassum horneri* for adsorption of cesium and strontium ions: equilibrium, kinetics, and mass transfer, Appl. Microbiol. Biotechnol. 103 (6) (2019) 2833–2843.
[22] Y. Hu, X. Guo, J. Wang, Biosorption of Sr^{2+} and Cs^{+} onto *Undaria pinnatifida*: Isothermal titration calorimetry and molecular dynamics simulation, J. Mol. Liq. 319 (2020), 114146.
[23] T.Y. Kim, J.E. Hong, H.M. Park, U.J. Lee, S.-Y. Lee, Decontamination of low-level contaminated water from radioactive cesium and cobalt using microalgae, J. Radioanal. Nucl. Chem. 323 (2020) 903–908.
[24] R. Yu, H. Chai, Z. Yu, X. Wu, Y. Liu, L. Shen, J. Li, J. Ye, D. Liu, T. Ma, et al., Behavior and mechanism of cesium biosorption from aqueous solution by living *Synechococcus* PCC7002, Microorganisms 8 (2020) 491.
[25] Y.-W. Chen, J.-L. Wang, Removal of cesium from radioactive wastewater using magnetic chitosan beads cross-linked with glutaraldehyde, Nucl. Sci. Tech. 27 (2016) 43.
[26] D. Yu, S. Morisada, H. Kawakita, K. Ohto, K. Inoue, X. Song, G. Zhang, Selective cesium adsorptive removal on using crosslinked tea leaves, Processes 7 (2019) 412.
[27] C.-H. Lee, W.-S. Chen, J.-Y. Wu, Lee, et al., Adsorption of cesium from waste desalination brine through Dowex G26 resin and comparison with t-BAMBP/kerosene and t-BAMBP/C(2)mimNTf(2) systems, Desalin. Water Treat. 236 (2021) 69–75.
[28] V.I. Gorshkov, V.A. Ivanov, I.V. Staina, Selectivity of phenol-formaldehyde resins and separation of rare alkali metals, React. Funct. Polym. 38 (1998) 157–176.
[29] V.V. Milyutin, V.M. Gelis, N.B. Leonov, Kinetics of sorption of cesium and strontium radionuclides on different sorbents, Radiochemistry 40 (1998) 431–433.
[30] I.M. Abdelmonem, E. Metwally, T.E. Siyam, F. Abou El-Nour, A.-R.-M. Mousa, Radiation synthesis of starch-acrylic acid-vinyl sulfonic acid/multiwalled carbon nanotubes composite for the removal of Cs-134 and Eu152+154 from aqueous solutions, J. Radioanal. Nucl. Chem. 319 (2019) 1145–1157.
[31] M.M.E. Breky, E.H. Borai, M.S.E. Sayed, M.M. Abo-Aly, Comparative sorption study of cesium, cobalt and europium using induced gamma radiation polymeric nanocomposites, Desalin. Water Treat. 116 (2018) 148–157.
[32] S.A. Erenturk, S. Haciyakupoglu, B.F. Senkal, Investigation of interaction behaviours of cesium and strontium ions with engineering barrier material to prevent leakage to environmental, J. Environ. Radioact. 213 (2020), 106101.
[33] A.M. James, S. Harding, T. Robshaw, N. Bramall, M.D. Ogden, R. Dawson, Selective environmental remediation of strontium and cesium using sulfonated hyper-cross-linked polymers (SHCPs), ACS Appl. Mater. Interfaces 11 (2019) 22464–22473.
[34] C.H. Ni, C.H. Yi, Z.Y. Feng, Studies of syntheses and adsorption properties of chelating resin from thiourea and formaldehyde, J. Appl. Polym. Sci. 82 (2001) 3127–3132.

[35] K.Z. Elwakeel, A. Shahat, Z.A. Khan, W. Alshitari, E. Guibal, Magnetic metal oxide-organic framework material for ultrasonic-assisted sorption of titan yellow and rose bengal from aqueous solutions, Chem. Eng. J. 392 (2020), 123635.
[36] D.D. Ristiana, S. Suyanta, N. Nuryono, Simple one-pot synthesis of sulfonic-acid-functionalized silica for effective catalytic esterification of levulinic acid, Indones. J. Chem. 22 (2022) 157–170.
[37] K.R. Benak, L. Dominguez, J. Economy, C.L. Mangun, Sulfonation of pyropolymeric fibers derived from phenol-formaldehyde resins, Carbon 40 (2002) 2323–2332.
[38] C. Tien, Adsorption Calculations and Modeling, Butterworth-Heinemann, Newton, MA, 1994, p. 243.
[39] Y.S. Ho, G. McKay, Pseudo-second order model for sorption processes, Process Biochemistry 34 (1999) 451–465.
[40] J. Crank, The Mathematics of Diffusion, 2nd. ed., Oxford University Press, Oxford, U.K., 1975, p. 414.
[41] G. Buema, N. Lupu, H. Chiriac, G. Ciobanu, R.D. Bucur, D. Bucur, L. Favier, M. Harja, Performance assessment of five adsorbents based on fly ash for removal of cadmium ions, J. Mol. Liq. 333 (2021), 115932.
[42] É.C. Lima, M.H. Dehghani, A. Guleria, F. Sher, R.R. Karri, G.L. Dotto, H.N. Tran, Chapter 3 - Adsorption: Fundamental aspects and applications of adsorption for effluent treatment, in: M. Hadi Dehghani, R. Karri, E. Lima (Eds.) Green Technologies for the Defluoridation of Water, Elsevier, 2021, pp. 41-88.
[43] O. Falyouna, O. Eljamal, I. Maamoun, A. Tahara, Y. Sugihara, Magnetic zeolite synthesis for efficient removal of cesium in a lab-scale continuous treatment system, J. Colloid Interface Sci. 571 (2020) 66–79.
[44] M. Thommes, K. Kaneko, A.V. Neimark, J.P. Olivier, F. Rodriguez-Reinoso, J. Rouquerol, K.S.W. Sing, Physisorption of gases, with special reference to the evaluation of surface area and pore size distribution (IUPAC Technical Report), Pure Appl. Chem. 87 (2015) 1051–1069.
[45] A.F. Shaaban, T.Y. Mohamed, D.A. Fadel, N.M. Bayomi, Removal of Ba(II) and Sr (II) ions using modified chitosan beads with pendent amidoxime moieties by batch and fixed bed column methods, Desalin. Water Treat. 82 (2017) 131–145.
[46] Y. Wei, K.A.M. Salih, S. Lu, M.F. Hamza, T. Fujita, T. Vincent, E. Guibal, Amidoxime functionalization of algal/polyethyleneimine beads for the sorption of Sr(II) from aqueous solutions, Molecules 24 (2019) 3893.
[47] T. Huang, L. Zhou, S.-W. Zhang, A. Li, Uptake of cesium by the hydroxysulfate green rust-modified composite aluminosilicate materials, mathematical modeling, and mechanisms, Colloids Surf., A 628 (2021), 127314.
[48] H.S. Hassan, M.F. Attallah, S.M. Yakout, Sorption characteristics of an economical sorbent material used for removal radioisotopes of cesium and europium, J. Radioanal. Nucl. Chem. 286 (2010) 17–26.
[49] P. Asgari, S.H. Mousavi, H. Aghayan, H. Ghasemi, T. Yousefi, Nd-BTC metal-organic framework (MOF); synthesis, characterization and investigation on its adsorption behavior toward cesium and strontium ions, Microchem. J. 150 (2019), 104188.
[50] S. Amin, S.A. Alavi, H. Aghayan, H. Yousefnia, Efficient adsorption of cesium using a novel composite inorganic ion-exchanger based on metal organic framework (Ni (BDC)(TED)) modified matal hexacyanoferrate, J. Organomet. Chem. 961 (2022), 122263.
[51] A.M. Friedman, J.W. Kennedy, The self-diffusion coefficients of potassium, cesium, iodide and chloride ions in aqueous solutions, JACS 77 (1955) 4499–4501.
[52] B.R. Figueiredo, D. Ananias, J. Rocha, C.M. Silva, Cs^+ ion exchange over lanthanide silicate Eu-AV-20: experimental measurement and modelling, Chem. Eng. J. 268 (2015) 208–218.
[53] F.A. Shehata, M.F. Attallah, E.H. Borai, M.A. Hilal, M.M. Abo-Aly, Sorption reaction mechanism of some hazardous radionuclides from mixed waste by impregnated crown ether onto polymeric resin, Appl. Radiat. Isot. 68 (2010) 239–249.
[54] H.N. Tran, E.C. Lima, R.-S. Juang, J.-C. Bollinger, H.-P. Chao, Thermodynamic parameters of liquid–phase adsorption process calculated from different equilibrium constants related to adsorption isotherms: a comparison study, J. Environ. Chem. Eng. 9 (6) (2021) 106674.
[55] O.A.A. Moamen, H.S. Hassan, W.F. Zaher, Taguchi L-16 optimization approach for simultaneous removal of Cs^+ and Sr^{2+} ions by a novel scavenger, Ecotoxicol. Environ. Saf. 189 (2020), 110013.
[56] S. Ai, Y. Huang, C. Huang, W. Yu, Z. Mao, Lead ion adsorption on functionalized sugarcane bagasse prepared by concerted oxidation and deprotonation, Environ. Sci. Pollut. Res. 28 (2021) 2728–2740.
[57] K. Li, M. Li, D. Xue, Solution-phase electronegativity scale: insight into the chemical behaviors of metal ions in solution, J. Phys. Chem. A 116 (2012) 4192–4198.
[58] R.G. Pearson, Acids and bases, Science 151 (1966) 172–177.
[59] V.V. Milyutin, P.G. Zelenin, P.V. Kozlov, M.B. Remizov, D.A. Kondrutskii, Sorption of cesium from alkaline solutions onto resorcinol-formaldehyde sorbents, Radiochemistry 61 (2019) 714–718.
[60] A.M. Metwally, M.M. Azab, A.A. Mahmoud, H.M. Ali, A.F. Shaaban, Core-shell polymer nanocomposite based on free radical copolymerization of anthranilic acid and o-amino phenol in the presence of copper hexacyanoferrates nanoparticles and its adsorption properties, J. Polym. Res. 29 (2022) 98.
[61] L.A. Attia, M.A. Youssef, O.A. Abdel Moamen, Feasibility of radioactive cesium and europium sorption using valorized *punica granatum* peel: kinetic and equilibrium aspects, Sep. Sci. Technol. 56 (2) (2021) 217–232.
[62] J. Li, Y. Zan, Z. Zhang, M. Dou, F. Wang, Prussian blue nanocubes decorated on nitrogen-doped hierarchically porous carbon network for efficient sorption of radioactive cesium, J. Hazard. Mater. 385 (2020), 121568.
[63] L. Lian, S. Zhang, N.a. Ma, W. Dai, Well-designed a novel phosphomolybdic-acid@PCN-224 composite with efficient simultaneously capture towards rubidium and cesium ions, Polyhedron 207 (2021) 115402.